8. K. M. Yamada and D. W. Kennedy, *J. Cell. Biochem.* **28**, 99 (1985).
9. S. K. Akiyama and K. M. Yamada, *J. Biol. Chem.* **260**, 10402 (1985).
10. C. R. Ill, E. Engvall, E. Ruoslahti, *J. Cell Biol.* **99**, 2140 (1984).
11. M. Ginsberg *et al., J. Biol. Chem.* **260**, 3931 (1985); D. M. Haverstick *et al., Blood* **66**, 496 (1985).
12. E. G. Hayman, M. D. Pierschbacher, E. Ruoslahti, *J. Cell Biol.* **100**, 1948 (1985).
13. S. K. Akiyama and K. M. Yamada, *J. Biol. Chem.* **260**, 4492 (1985).
14. J.-C. Boucaut *et al., J. Cell Biol.* **99**, 1822 (1984).
15. K. Nagata and Y. Ichikawa, *J. Cell. Physiol.* **98**, 167 (1979).
16. I. J. Fidler, *J. Natl. Cancer Inst.* **45**, 773 (1970).
17. L. A. Liotta and C. DeLisi, *Cancer Res.* **37**, 4003 (1977).
18. I. J. Fidler, *Eur. J. Cancer* **9**, 223 (1973); L. A. Liotta, J. Kleinerman, G. M. Saidel, *Cancer Res.* **36**, 889 (1976); G. T. Gasic, *Cancer Metastasis Rev.* **3**, 99 (1984).
19. V. A. Najjar and M. Fridkin, Eds., *Ann. N.Y. Acad. Sci.* **419**, 1 (1983).
20. I. J. Fidler, *Nature (London) New Biol.* **242**, 148 (1973).
21. ———, *Cancer Res.* **34**, 1074 (1974).
22. ———, *Methods Cancer Res.* **15**, 399 (1978).

23. We thank I. J. Fidler of the M. D. Anderson Hospital, University of Texas, Houston, TX, for providing B16-F10 cells. Supported in part by grant CA-34918 from the U.S. Public Health Service to K. Olden.

2 October 1985; accepted 19 May 1986

A Wind-Forced Ekman Spiral as a Good Statistical Fit to Low-Frequency Currents in a Coastal Strait

MICHAEL W. STACEY, STEPHEN POND, PAUL H. LEBLOND

Ekman's classical analysis of wind-driven currents is a fundamental component of the modern circulation theory of the oceans, but there have been few good observations of the predicted Ekman spiral, where the velocity vector rotates clockwise in direction (in the Northern Hemisphere) and decays exponentially in magnitude with increasing depth. An analysis of recent cyclesonde velocity measurements based on the use of empirical orthogonal functions, however, suggests that a classical Ekman spiral was a good statistical fit to a significant portion of the low-frequency current fluctuations in the Strait of Georgia, British Columbia, for fluctuation periods of about 5 to 10 days.

THE RESPONSE OF THE OCEAN TO the forcing of the wind was first analyzed theoretically in 1905 by Ekman (*1*), who assumed (i) an infinitely wide, steady-state ocean with no horizontal variations and (ii) a constant eddy viscosity to distribute momentum into the water column. The basic predictions of the analysis, that the surface current veers to the right of the wind (in the Northern Hemisphere) and decreases in amplitude with depth, are generally accepted, but, because of the assumptions and a lack of reliable observations (*2*), the details generally are not. An empirical orthogonal function analysis of the low-frequency current fluctuations at a cyclesonde, that is, a profiling current meter, moored in the Strait of Georgia, British Columbia, however, suggests that during the observation period a classical Ekman spiral was an accurate representation of much of the actual flow field. To our knowledge, the results described here are the most supportive of any to date of Ekman's simple theory, particularly because they apply to an ensemble of realizations, taken over a period of several months, and because they show a good fit to the vertical variation in the horizontal currents over a depth of over 100 m.

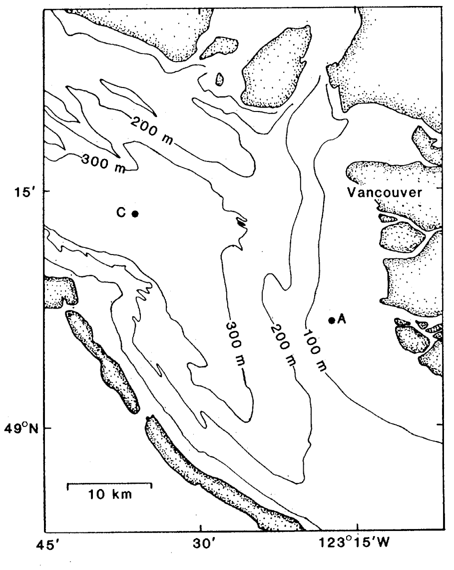

Fig. 1. Plan view of the Strait of Georgia, showing the cyclesonde (C) and anemometer (A) stations. The anemometer is located 18 m above sea level.

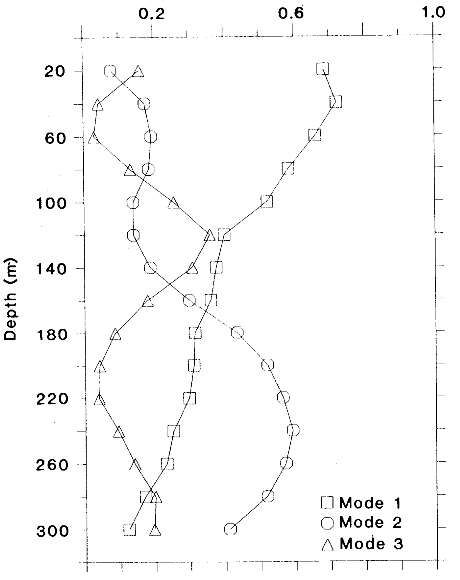

Fig. 2. The fraction of the variance explained by the first three orthogonal modes as a function of depth.

The locations of the cyclesonde mooring and the anemometer station are shown in Fig. 1. Deployed from 20 June 1984 until 14 January 1985, the cyclesonde was set to profile to within 20 m of the surface and to a depth of 300 m in a total water depth of 370 m. These data allowed the synthesis of 15 discrete velocity time series at 20-m intervals (*3*). The east-west and north-south velocity components of the currents and the wind were low-pass filtered by applying a 25-hour running mean three times successively. The filter passes approximately 80% of the amplitude at 0.2 cycle per day, approximately 95% at 0.1 cycle per day. The filtered time series were then resampled at 6-hour intervals. Autospectra of the filtered currents showed that the dominant periods of the fluctuations were greater than 5 days.

Two-dimensional, that is, complex empirical orthogonal, functions (*4*) were calculated from the current velocity time series (with the mean removed). Figure 2 shows the variance accounted for by the first three orthogonal modes as a function of depth. The first three modes together account for 89% of the total variance. Mode 1 dominates the variance from 20 to 160 m. Figure 3 shows the mode 1 eigenfunction. The dots in Fig. 3 locate the tips of the orthogonal, horizontal velocity vectors ($\mathbf{U}, \mathbf{V}$) of a classical Ekman spiral, given by

$$\mathbf{U} = \mathbf{V}_0 \cos\left(\frac{\pi}{4} + \frac{\pi z}{D_E}\right) \exp\left(\frac{\pi z}{D_E}\right)$$

$$\mathbf{V} = \mathbf{V}_0 \sin\left(\frac{\pi}{4} + \frac{\pi z}{D_E}\right) \exp\left(\frac{\pi z}{D_E}\right)$$

where the z-axis is directed upward and equals zero at the ocean's surface (*5*). $\mathbf{U}$ and

---

Department of Oceanography, University of British Columbia, Vancouver, British Columbia, Canada V6T 1W5.

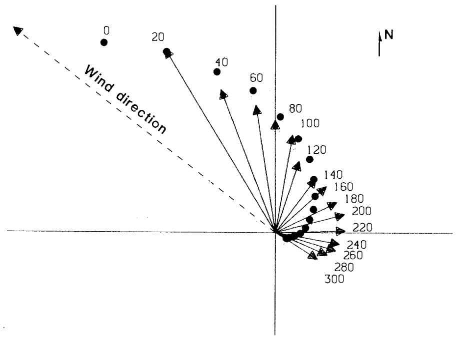

Fig. 3. The mode 1 eigenfunction. Its direction has been fixed by picking the arrow at 20 m to lie along the direction of the principal axis of the covariance matrix of the currents at 20 m. The dots show the amplitude and direction as given by the Ekman spiral. The wind direction is the direction of the principal axis of the covariance matrix of the wind.

V are measured relative to a coordinate system that has been rotated to make the Ekman spiral match the eigenfunction. The Ekman depth D_E has been set equal to 325 m, and $\mathbf{V}_0$ equals 0.66 in nondimensional units (*6*). The amplitude is about 10 cm $\sec^{-1}$ at 20 m, which is about 3% of the wind amplitude. The eddy viscosity, calculated from D_E (*5*), is 5300 $\text{cm}^2 \sec^{-1}$. The mode 1 eigenfunction, over the depth range for which it dominates the variance, is in close quantitative agreement with the classical Ekman spiral. This strongly suggests that Ekman's theory is the appropriate dynamical explanation in this region. Below about 160 m, where the eigenfunction no longer dominates the variance, the Ekman spiral predicts amplitudes that are substantially less than those of the eigenfunction. There is evidence of strong tidal currents in the strait (they are in fact much more energetic than the wind-forced flow at depth) (*3*), so possibly the Ekman spiral has been modified by the interaction of the wind-forced and tidally forced motions, the modification being most noticeable at depth because that is where the tides are dominant. The presence of strong tides may also explain why the Ekman depth is larger than commonly found in the open ocean. Tidally generated turbulence may increase the depth to which wind-generated momentum can diffuse.

The direction of the principal axis of the covariance matrix of the wind, relative to that of the currents at 20 m (which is the assumed direction at 20 m of the mode 1 eigenfunction), is also shown in Fig. 3. As the simple theory predicts, the current is deflected to the right of the wind. The deflection is much less than the 45° predicted by Ekman's theory, but such a deviation is expected when there is a logarithmic, oceanic boundary layer near the ocean's surface (*7*). Also, the near-surface current profile may be substantially influenced by the tendency of the water column to become more stratified as the surface is approached. The Brunt-Vaisala frequency,

$$N = \left(\frac{-g}{\rho}\,\frac{\partial \rho}{\partial z}\right)^{1/2}$$

where g is the acceleration due to gravity and ρ is the water density, is a measure of the degree of stability of the water column (*8*) and can decrease from as much as 0.1 $\sec^{-1}$ near the surface, when there is overlying freshwater from river runoff, to about 0.02 $\sec^{-1}$ at 20 m. From 20 to 300 m it decreases to about 0.005 $\sec^{-1}$.

According to Ekman's theory, in the Northern Hemisphere the depth-integrated transport is 90° to the right of the surface wind, independent of the eddy viscosity. The calculated transport, determined from the eigenfunction, is 79° to the right of the measured wind. This small discrepancy could be caused by a number of factors. Five possibilities are (i) the influence of the tides on the eigenfunction, (ii) the fact that the eigenfunction could not be calculated over the entire depth of the water column, (iii) the horizontal distance separating the cyclesonde and the anemometer (Fig. 1), (iv) topographic effects, and (v) differences between the directions of the wind and the eigenfunction and the directions of the principal axes of the covariance matrices.

The inner rotary cross-spectrum (*9*) of the wind with the time-dependent part of the mode 1 eigenfunction (Fig. 4) shows that the clockwise rotating components of each vector series are coherent over a broad range of frequencies (from about 0.1 to 0.2 cycle per day). The outer rotary cross-spectrum (Fig. 4) shows that the anticlockwise rotating component of the eigenfunction is also coherent with the clockwise rotating component of the wind. The autospectrum of the wind shows that the clockwise rotating component is about twice as energetic as the anticlockwise rotating component over the range of frequencies for which there is coherence with the eigenfunction; presumably this is why it is more coherent with the eigenfunction. Over the entire frequency range for which the eigenfunction has substantial energy, both components of the eigenfunction are coherent with the wind, except at frequencies less than about 0.08 cycle per day where the eigenfunction has energetic fluctuations that are not highly coherent with the wind. The fluctuations at those frequencies are caused primarily by the

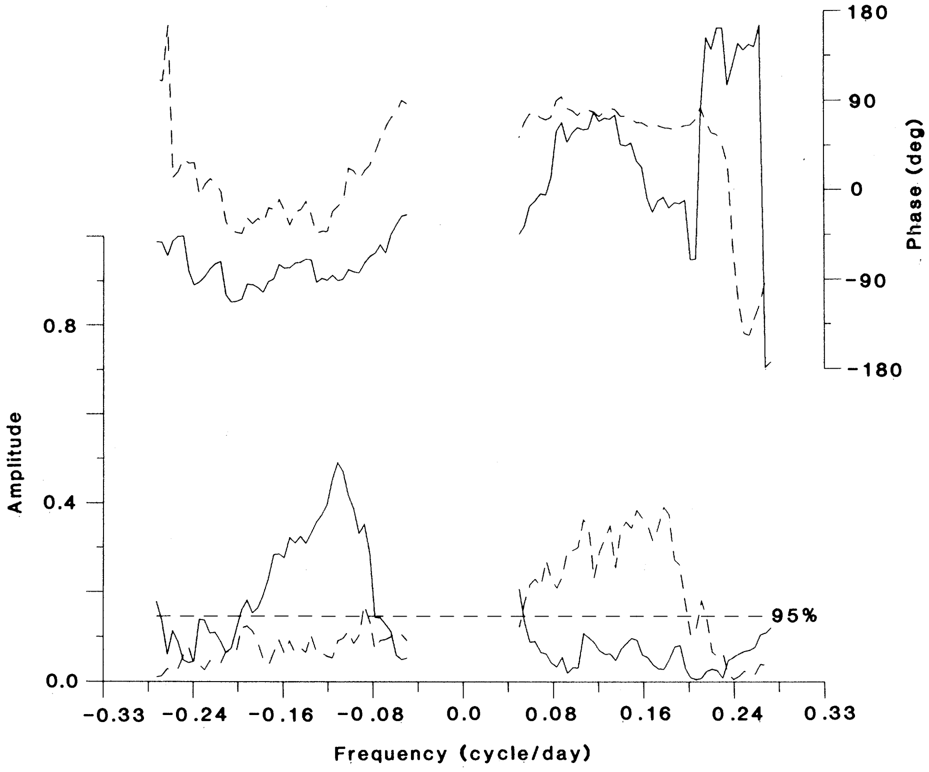

Fig. 4. The inner coherency squared (solid lines) and outer coherency squared (dashed lines) of the wind and the mode 1 eigenfunction. For the inner coherency, the negative frequencies give the coherency squared of the clockwise rotating components of each vector series; the positive frequencies give the coherency squared of the anticlockwise rotating components. For the outer coherency, the negative frequencies give the coherency squared of the anticlockwise rotating component of the wind and clockwise rotating component of the eigenfunction; the positive frequencies give the coherency squared of the clockwise rotating component of the wind and anticlockwise rotating component of the eigenfunction. The horizontal dashed line indicates the 95% confidence limit for noise.

tides, particularly the MSf (0.068 cycle per day) tidal constituent (*3*). That is, the wind-forced and tidally forced motions interact nonlinearly, and so some tidal energy has leaked into the eigenfunction described here. This may at least partially explain the modification to the Ekman spiral at depth that was described earlier. For both the clockwise and anticlockwise rotating components of the eigenfunction, at all frequencies for which the eigenfunction is coherent with the wind the magnitude of the phase is close to 90°, so the lag in time is a function of frequency. At the frequency for which the eigenfunction is most coherent with the wind ($\simeq -0.12$ cycle per day), the lag time is about 2 days, which corresponds to about three inertial periods at 49° latitude.

These results suggest that a substantial portion of the observed low-frequency fluctuations in the Strait of Georgia were, on average, interpretable as a quasi-steady, classical Ekman spiral. The low frequency of the fluctuations relative to the inertial period of 16 hours suggests that the quasi-steady assumption was valid. The presence of significant tidal currents in the strait suggests that the distribution of turbulence with depth was more uniform than if only the wind-forced flow had been present; thus the assumption of constant eddy viscosity had a better chance of being approximately satisfied. The fluctuating nature of the flow made the assumptions of infinite expanse and no horizontal variations reasonable approximations. More importantly, by examining the fluctuations over a number of cycles instead of examining the mean flow, we obtain a result that is an average of a number of separate realizations.

In general, contemporary wisdom states that Ekman's theory is not sophisticated enough to explain actual flow fields. The results presented here show that Ekman's theory can in certain cases describe in some detail the vertical structure of wind-forced flows, even in hydrographically complicated regions such as coastal straits.

REFERENCES AND NOTES

1. V. W. Ekman, *Ark. Mat. Astron. Fys.* **2** (No. 11), 52 (1905).
2. Previous observations of Ekman spirals include the following: J. Gonella, *C. R. Acad. Sci. Ser. B* **266**, 205 (1968); K. Hunkins, *Deep Sea Res.* **13**, 607 (1966); R. A. Weller, *J. Geophys. Res.* **86**, 1969 (1981).
3. M. W. Stacey, S. Pond, P. H. LeBlond, H. J. Freeland, D. M. Farmer, in preparation.
4. P. K. Kundu and J. S. Allen, *J. Phys. Oceanogr.* **6**, 181 (1976).
5. S. Pond and G. L. Pickard, *Introductory Dynamical Oceanography* (Pergamon, Elmsford, NY, 1983). This formulation assumes that the water is infinitely deep. For Ekman depths D_E less than the depth of the water column, taking the bottom boundary into account results in only a minor modification.
6. D_E was chosen to give the observed decay in velocity with depth; V_0 to make the eigenfunction and Ekman spiral agree at 20 m.
7. H. Tennekes and J. L. Lumley, *A First Course in Turbulence* (MIT Press, Cambridge, MA, 1972).
8. A. E. Gill, *Atmosphere-Ocean Dynamics* (Academic Press, New York, 1982).
9. C. N. K. Mooers, *Deep Sea Res.* **20**, 1129 (1973).
10. Supported by Natural Sciences and Engineering Research Council of Canada strategic grant A1108. We thank the officers and crew of the CSS *Vector* for their assistance with the mooring work and V. Lee for assistance with the data analysis.

27 January 1986; accepted 30 April 1986

A Poliovirus Neutralization Epitope Expressed on Hybrid Hepatitis B Surface Antigen Particles

F. DELPEYROUX, N. CHENCINER, A. LIM, Y. MALPIÈCE, B. BLONDEL, R. CRAINIC, S. VAN DER WERF, R. E. STREECK*

The hepatitis B virus (HBV) envelope protein carrying the surface antigen (HBsAg) is assembled with cellular lipids in mammalian cells into empty viral envelopes. In a study to evaluate the capacity of such particles to present foreign peptide sequences in a biologically active form, in-phase insertions were created in the S gene encoding the major envelope protein. One of the sequences inserted was a synthetic DNA fragment encoding a poliovirus neutralization epitope. Mammalian cells expressing the modified gene secreted hybrid particles closely resembling authentic 22-nanometer HBsAg particles. These particles reacted with a poliovirus-specific monoclonal antibody and induced neutralizing antibodies against poliovirus. The results indicate that empty viral envelopes of HBV may provide a means for the presentation of peptide sequences and for their export from mammalian cells.

VARIOUS PARTICLES ARE PRESENT in the blood of humans infected with the hepatitis B virus (HBV), including 45-nm particles corresponding to complete virions and spherical or tubular particles, about 22 nm in diameter, corresponding to empty viral envelopes (*1*). The 22-nm spherical particle is a complex structure containing lipids and about 100 molecules of protein, including a major protein carrying the surface antigen (HBsAg) encoded by the S gene, and a minor protein encoded by the pre-S region and the S gene (*2, 3*). Both the major and the minor protein are found in glycosylated and nonglycosylated form. The pre-S region codes for an immunodominant epitope of HBV (*4*), but only the 226-amino-acid sequence of the major envelope protein is needed for the assembly of the 22-nm particles and their secretion from mammalian cells (*5*). HBsAg particles from chronic carriers of HBV are currently used as vaccine against hepatitis B (*1*); they are also synthesized and secreted by mammalian cell lines transfected by vectors carrying the S gene (*6, 7*). Related particles have been prepared from yeast (*8*).

We have developed a cellular system for synthesizing HBsAg and have used it for studying the structural requirements for formation and secretion of 22-nm particles by creating in-phase insertions of variable length and sequence in different regions of the S gene (*9*).

The plasmid pPAP (Fig. 1A) carries the SV40 early promoter and a modified S gene encoding an envelope protein (HBsPolioAg) that is 13 amino acid residues longer than HBsAg. The construction of this plasmid was achieved by inserting a 39-bp oligonucleotide into a naturally occurring Bam HI site; this led to duplication of amino acids 112–113 (Gly–Ser) and insertion of an 11-amino-acid sequence between the duplicated residues. The site of insertion into HBsAg is part of a hydrophilic domain of the viral envelope protein and is close to the region carrying most of the HBs antigenic determinants (*1*). We also constructed a plasmid termed pLAS, which is identical to pPAP except for the insertion in the Bam HI site (Fig. 1A). The inserted sequence represents amino acid residues 93–103 of capsid protein VP1 of poliovirus type 1 (Mahoney strain). The corresponding synthetic peptide mimicks a neutralization epitope of infectious poliovirus (*10*) and can be recognized by a neutralizing monoclonal antibody (C3) (*11*).

Clones of mouse L cells transfected by

F. Delpeyroux, N. Chenciner, A. Lim, Y. Malpièce, R. E. Streeck, Unité des Applications du Génie Génétique (G3), Institut Pasteur, 75724 Paris Cedex 15, France.
B. Blondel and R. Crainic, Unité de Virologie Médicale, Institut Pasteur, 75724 Paris Cedex 15, France.
S. Van der Werf, Unité de Virologie Moléculaire, Institut Pasteur, 75724 Paris Cedex 15, France.

*To whom correspondence should be addressed.